

Heat kernel and intrinsic Gaussian processes on manifolds

BY KE YE

KLMM, Academy of Mathematics and Systems Science, Chinese Academy of Sciences, China
keyk@amss.ac.cn

MU NIU

School of Mathematics and Statistics, University of Glasgow, U.K.
mu.niu@glasgow.ac.uk

POKMAN CHEUNG

London, U.K.
pokman@alumni.stanford.edu

SUMMARY

There is an increasing interest in the problem of nonparametric regression like Gaussian processes with predictors locating on manifold. Some recent researches developed intrinsic Gaussian processes by using the transition density of the Brownian motion on submanifolds of \mathbb{R}^2 and \mathbb{R}^3 to approximate the heat kernels. However, when the dimension of a manifold is bigger than two, the existing method struggled to get good estimation of the heat kernel. In this work, we propose an intrinsic approach of constructing the Gaussian process on general manifolds such as orthogonal groups, unitary groups, Stiefel manifolds and Grassmannian manifolds. The heat kernel is estimated by simulating Brownian motion sample paths via the exponential map, which does not depend on the embedding of the manifold. To be more precise, this intrinsic method has the following features: (i) it is effective for high dimensional manifolds; (ii) it is applicable to arbitrary manifolds; (iii) it does not require the global parametrisation or embedding which may introduce redundant parameters; (iv) results obtained by this method do not depend on the ambient space of the manifold. Based on this method, we propose the ball algorithm for arbitrary manifolds and the strip algorithm for manifolds with extra symmetries, which is both theoretically proven and numerically tested to be much more efficient than the ball algorithm. A regression example on the projective space of dimension eight is given in this work, which demonstrates that our intrinsic method for Gaussian process is practically effective in great generality.

Some key words: Intrinsic; Manifolds; Heat kernel; Gaussian process; Brownian motion.

1. INTRODUCTION

Due to the high dimensionality and non-linearity of data, modelling problems on Euclidean spaces is no longer always efficient and satisfied. This provides an impetus for mathematicians and statisticians to develop new theories and methods to model problems on more general spaces, which are manifolds. There is an enormous amount of practical problems which can be naturally modelled on various manifolds and efficiently studied by statistics on them. In this work we focus on matrix manifolds which are widely used in pattern recognition, ecology, medical and biolog-

ical science. For example, medial models of the human kidney can be studied by the statistics of Lie groups Fletcher et al. (2003); palaeomagnetic data sets are modelled and analysed on spheres Gidskehaug (1976); new algorithms for problems of pedestrian detection and object categorization are proposed through the investigation of the space of positive definite matrices Jayasumana et al. (2013); biological and medical images are considered as points in shape spaces Bookstein (2013); Kendall (1977); clustering algorithms on Stiefel manifolds and Grassmannian manifolds are applied to image and video recognition problems Chikuse (2012); Turaga et al. (2011). On the other hand, as one of the most prominent methods, the Gaussian process (GP) has been extensively used in statistics and machine learning on Euclidean spaces Rasmussen (2004). However, it can not be directly generalized to model data on a general manifold. A major challenge in constructing Gaussian processes on manifolds is choosing a valid covariance kernel. This is a non-trivial problem and most of the focus has been on developing covariance kernels specific to a particular manifold Jayasumana et al. (2016); Lafferty & Lebanon (2005); Jayasumana et al. (2013). In Lin et al. (2018), an extrinsic Gaussian process is proposed on manifolds by first embedding the manifolds into higher-dimensional Euclidean spaces. The well known squared exponential kernel can then be applied on the images after embedding. However, such embeddings are not always available or easy to obtain for general manifolds. Even if the embedding exists, the dimension of the embedded Euclidean space could be much higher than the original manifold. The embedding of Grassmannians Lin et al. (2018) is such an example. Readers can also find an example in section 5.2 where the dimension of the manifold is 8 but the dimension of the embedded space is 25. Castillo et al. (2014) instead proposes to use randomly rescaled solutions of the heat equation to define a valid covariance kernel for reasonably a broad class of compact manifolds. However, the proposed heat kernels are computationally intractable, and authors of Castillo et al. (2014) did not provide the implementation of their approach in practice.

Niu et al. (2018) proposes a novel class of intrinsic Gaussian processes (in-GPs) which refers to a Gaussian process that employs the intrinsic Riemannian geometry of the manifold. Niu et al. (2018) develop a practical and general in-GP methodology, which uses heat kernels as covariance kernels. The heat kernel generalizes the popular and well-studied squared exponential kernel (also known as RBF kernel) to the Riemannian manifold, which arises from the Laplace operator and thus fully exploits the intrinsic geometry of the manifold. They utilise connections between heat kernels and transition densities of the Brownian motion on manifolds to obtain algorithms for approximating covariance kernels.

Manifolds considered in Niu et al. (2018) are mainly subsets of \mathbb{R}^2 and \mathbb{R}^3 . In this paper, we will consider a more general manifolds such as Lie groups and their homogeneous spaces, including orthogonal groups, Stiefel manifolds and Grassmannian manifolds. We list in Table 1 the manifolds which are discussed in this paper. Basic facts about Lie groups and homogeneous spaces are provided in the Appendix A.

The approach of Niu et al. (2018) requires the parameterisation of the manifold so that the induced metric tensor can be derived from the local coordinates. The associated Laplace-Beltrami operator Δ_s of the Riemannian manifold can be defined. The Laplace-Beltrami operator is also the infinitesimal generator of the Brownian motion on the manifold. The Brownian motion on a Riemannian manifold in a local coordinate system is given by a system of stochastic differential equations (SDE) in the Ito form Hsu (1988, 2008). To simulate the Brownian motion sample paths, Niu et al. (2018) discretises the SDE in Hsu (1988, 2008) using the Euler-Maruyama method (Kloeden & Platen (1992)). There is no issue with the SDE in its infinitesimal form. However, when it is approximated by a discretisation, the accuracy of this approximation is strongly related to the choices parameterisation. In this paper, we present a method of simulating

the Brownian motion on a Riemannian manifold by exponential maps which do not require the parametrisation of the manifold. Detailed discussions are in Section 2.2 and Section 4.

Niu et al. (2018) estimates the transition probability of the Brownian motion by counting the number of sample paths reaching the neighbourhood of the target point which is a ball with a small radius. We refer this method as the ball algorithm. It could be problematic when the dimension of the manifold is high, since the probability of the Brownian motion sample paths reaching a small ball centred on a given point could tends to zero as the dimension of the manifold increases. We developed a new approach referred as the strip algorithm in Section 3.2 to estimate the transition density of the Brownian motion. It is capable of dealing with higher dimensional manifolds. The comparison between these two algorithms is given in Section 3.3.

2. INTRINSIC GAUSSIAN PROCESS ON MANIFOLDS

2.1. Background

Let M be a m -dimensional complete Riemannian manifold and let $\mathcal{D} = \{(x_i, y_i), i = 1, \dots, n\}$ be the data, with n the number of observations, $x_i \in M$ the predictor or location value of observation i and y_i the corresponding response variable. We would like to do inferences on how the output y varies with the input x , including the prediction of the y -value at a new location x_* , which is not represented in the training dataset. Assuming Gaussian noise and a simple measurement structure, we let

$$y_i = f(x_i) + \epsilon_i, \quad \epsilon_i \sim \mathcal{N}(0, \sigma_{noise}^2), \quad x_i \in M, \quad (1)$$

where σ_{noise}^2 is the variance of the noise.

Following the idea of Niu et al. (2018), we can place an Gaussian processes prior for the unknown function $f : M \rightarrow \mathbb{R}$, we have

$$p(\mathbf{f}|x_1, x_2, \dots, x_n) = \mathcal{N}(\mathbf{0}, \Sigma), \quad (2)$$

where \mathbf{f} is a vector containing the realisations of $f(\cdot)$ at the sample points x_1, \dots, x_n , $f_i = f(x_i)$, and Σ is the covariance matrix of these realisations induced by the in-GP covariance kernel. The heat kernel $p_t^M(x, y)$ is used as the covariance kernel, where the time parameter t of p_t^M has the same effect as that of the length-scale parameter of the RBF kernel, controlling the rate of decay of the covariance. In particular, the entries of Σ are obtained by evaluating the covariance kernel at each pair of locations, that is,

$$\Sigma_{ij} = \sigma_h^2 p_t^M(x_i, x_j). \quad (3)$$

The hyperparameter σ_h^2 allows rescaling the heat kernel for extra flexibility. Following standard practice for GPs, this prior distribution is updated with information in the response data to obtain a posterior distribution. The posterior distribution of f evaluated at locations $\mathbf{X} = (x_1, \dots, x_n)$ has the following form:

$$\begin{aligned} f(x)|\mathcal{D} &\sim GP(m_{post}, \Sigma_{post}) \\ m_{post} &= \Sigma_{x, \mathbf{X}} (\Sigma_{\mathbf{X}, \mathbf{X}} + \sigma_{noise}^2 \mathbf{I})^{-1} \mathbf{y} \\ \Sigma_{post} &= \Sigma_{x, x} - \Sigma_{x, \mathbf{X}} (\Sigma_{\mathbf{X}, \mathbf{X}} + \sigma_{noise}^2 \mathbf{I})^{-1} \Sigma_{\mathbf{X}, \mathbf{X}}, \end{aligned}$$

where $\mathbf{y} = (y_1, \dots, y_n)$. Let \mathbf{f}_* be a vector of values of f at test points which are not in the training sample. The joint distribution of \mathbf{f} and \mathbf{f}_* is multivariate normal. The predictive distribution

$p(\mathbf{f}_*|\mathbf{y})$ is derived by marginalizing out \mathbf{f} . Namely,

$$p(\mathbf{f}_*|\mathbf{y}) = \int p(\mathbf{f}_*\mathbf{f}|\mathbf{y})d\mathbf{f} = \mathcal{N}(\Sigma_{\mathbf{f}_*\mathbf{f}}(\Sigma_{\mathbf{f}\mathbf{f}} + \sigma_{noise}^2 I)^{-1}\mathbf{y}, \Sigma_{\mathbf{f}_*\mathbf{f}_*} - (\Sigma_{\mathbf{f}\mathbf{f}} + \sigma_{noise}^2 I)^{-1}\Sigma_{\mathbf{f}\mathbf{f}_*}).$$

The key challenge for inference using in-GPs is how to get the heat kernel $p_t^M(x, y)$. Let Δ_s be the Laplacian-Beltrami operator on M , and δ the Dirac delta function. A heat kernel of M is a smooth function $p_t^M(x, y)$ on $M \times M \times \mathbb{R}^+$ that satisfies the heat equation:

$$\frac{\partial}{\partial t}p_t^M(x_0, x) = \frac{1}{2}\Delta_s p_t^M(x_0, x), \quad (4)$$

$$\lim_{t \rightarrow 0} p_0^M(x_0, x) = \delta(x_0, x), \quad x_0, x \in M. \quad (5)$$

Here the initial condition holds in the distributional sense Berline et al. (2003). If M is a Euclidean space \mathbb{R}^d , the heat kernel has a closed form expression corresponding to time varying Gaussian function:

$$p_t^M(\mathbf{x}_0, \mathbf{x}) = \frac{1}{(2\pi t)^{d/2}} \exp\left\{-\frac{\|\mathbf{x}_0 - \mathbf{x}\|^2}{2t}\right\}, \quad \mathbf{x} \in \mathbb{R}^d.$$

The heat kernel of \mathbb{R}^d can be seen as the scaled version of RBF kernel (or squared exponential kernel).

The closed form expressions for p_t^M do not exist for general Riemannian manifolds. Explicit solutions are available only for very special cases, such as Euclidean spaces. Therefore, for most cases, one can not explicitly evaluate p_t^M or the corresponding covariance matrices. To overcome this challenge and bypass the need to solve the heat equation (4) and (5) directly, we utilise the fact that the heat kernel on M can be interpreted as the transition density of the Brownian motion.

Similar to Niu et al. (2018), we estimate the heat kernel $p_t^M(x_i, x_j)$ for a pair (x_i, x_j) by simulating the Brownian motion on M and numerically evaluate the transition density of the Brownian motion. However, unlike the method in Niu et al. (2018), here we do not require an explicit parametrisation of the manifold. Also manifolds considered in Section 4 are not just simple subsets of \mathbb{R}^2 and \mathbb{R}^3 . The simulation of the Brownian motion on a Riemannian manifold is discussed in Section 2.2 and the detailed algorithms are given in Section 4 for different types of manifolds respectively.

2.2. Simulation of the Brownian motion on a Riemannian manifold

The goal of this subsection is to recall a method of simulating the Brownian motion on a Riemannian manifold by exponential maps, which was first proposed in McKean et al. (1960) for Lie groups and later generalized to arbitrary Riemannian manifolds in Gangolli (1964). Let (M, g) be an m -dimensional Riemannian manifold with metric g and let x be a point on M . We denote by $T_x M$ the tangent space of M at x , $W_x(\delta)$ a Brownian motion step with step variance δ in $T_x M$ from the origin and $\exp_x : U_x \rightarrow M$ the exponential map from an open neighborhood $U_x \subseteq T_x M \simeq \mathbb{R}^d$ around the origin. We have Algorithm 1 to numerically simulate a Brownian motion sample path on M .

The following fact ensures that \mathbf{B}_{x_0} obtained in Algorithm 1 is indeed a numerical approximation of a Brownian motion sample path on (M, g) .

THEOREM 1. (Gangolli, 1964, Theorem 4.1) *The path \mathbf{B}_{x_0} converges to a Brownian sample path on M with probability 1, as $\delta \rightarrow 0$.*

We remark that in practice the main difficulty of applying Algorithm 1 to simulate Brownian motion sample paths is that in general, the exponential map on (M, g) is not explicitly known.

Algorithm 1. Simulation of the Brownian motion on a Riemannian manifold

Initialize $x_0 = x$ and $B_{x_0}(0) = x_0$, t is the diffusion time, and $T = t/\delta$ is the number of Brownian motion steps.

For $j = 1, 2, \dots, T$

 compute $W_{x_{j-1}}(\delta)$; (Brownian motion sample path in $U_{x_{j-1}}$ with step variance δ)

 compute $B_{x_0}(j\delta) = \exp(W_{x_{j-1}}(\delta))$; (one-step BM sample path from x_{j-1} on M)

 set $x_j = B_{x_0}(j\delta)$;

set $\mathbf{B}_{x_0} = \{B_{x_0}(0), B_{x_0}(\delta), B_{x_0}(2\delta), \dots, B_{x_0}(t)\}$; (BM sample path from x_0 on M)

However, we will see in the sequel that for the Riemannian manifolds considered in this paper such as Lie groups and their homogeneous spaces, Algorithm 1 is a convenient and efficient way to simulate Brownian motion sample paths. Detailed algorithms of simulating the Brownian motion on different types of manifolds are given in Section 4. In order to compare Algorithm 1 with the method using stochastic differential equation in Niu et al. (2018), we consider the example of the standard sphere parametrised by latitude ϕ and longitude θ in details. This coordinate system cannot cover the north and south poles – they are the singularities. In this coordinate system, the Brownian motion in Niu et al. (2018) is described by

$$(d\phi, d\theta) = \left(-\frac{\tan(\phi)}{2}dt + dB_\theta, \frac{1}{\cos(\phi)}dB_\phi\right).$$

Note that near the poles the drift velocity $(-\tan(\phi)/2, 0)$ becomes large and points away from the poles (huge repulsive drift); There is no issue with the stochastic differential equation in its infinitesimal form. However, when it is approximated by a discretisation, near the poles the drift term may become too large for the simulated step to be a good approximation of the actual Brownian motion. However in our approach, the simulation of Brownian Motion does not require the parametrisation of the space and hence we do not have such a problem at the poles.

3. ESTIMATE THE HEAT KERNEL FROM BROWNIAN MOTION SAMPLE PATHS

To explore the connection between the heat kernel and the Brownian motion on a manifold, we let $B_{x_0}(t)$ be the Brownian motion on M starting from $x_0 = B_{x_0}(0)$. The transition probability of $B_{x_0}(t) \in D \subseteq M$ at time t , for any Borel set D , is given by

$$\mathbb{P}[B_{x_0}(t) \in D \mid B_{x_0}(0) = x_0] = \int_D p_t^M(x_0, x) dx, \quad (6)$$

where the integral is defined with respect to the volume form of M . In Niu et al. (2018), authors estimate the heat kernel on a given manifold via approximating the integral in (6) by simulating the Brownian motion sample paths and numerically evaluating the transition probability. In the rest of this section, we will discuss how to efficiently simulate Brownian motion sample paths on manifolds by two methods of numerical differential geometry.

3.1. Ball algorithm

We first recall from Niu et al. (2018) that the transition probability in (6) can be approximated by counting the number of sample paths reaching the neighbourhood of the target point. We refer to it as the ball method. Let $\{B_x(t) : t > 0\}$ be the Brownian motion on M with starting point $B_x(0) = x$, $x \in M$ and let N be the number of simulated sample paths. For $t > 0$ and $y \in M$ the probability of $B_x(t)$ in a small neighbourhood D of y can be estimated by counting how many Brownian motion sample paths reach D at time t . An illustrative diagram is shown in Figure

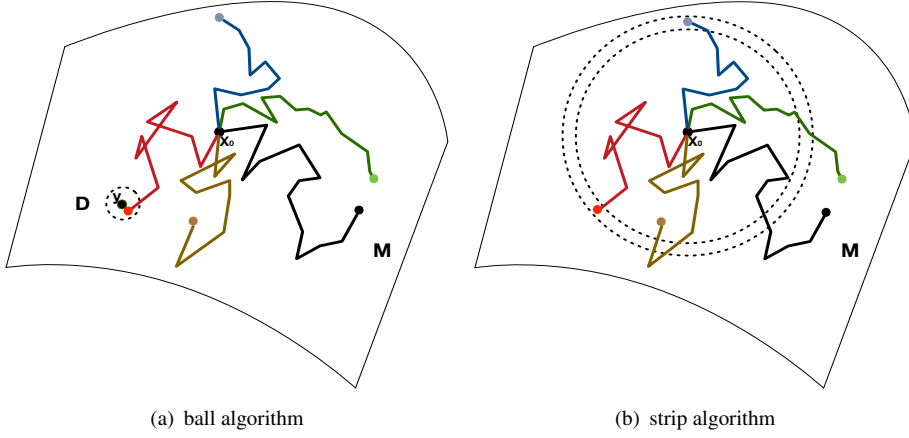


Fig. 1. Illustrative examples of the Brownian motion on manifold M . Five independent Brownian motion sample paths from time 0 to t represented by the solid coloured lines in both 1(a) and 1(b). x_0 is the starting point of Brownian motion sample paths. In 1(a) only one sample path (red) reaches D at time t , so the transition probability is $1/5$. In 1(b) there are two sample paths (red and blue) reach the strip at time t so the transition probability is $2/5$.

1(a). The transition density is approximated by

$$p_t^M(x, y) \approx \frac{1}{\text{Vol}(D)} \frac{k}{N}, \quad (7)$$

where $\text{Vol}(D)$ is the volume of D and k is the number of Brownian motion sample paths falling into D at time t . Based on (7) and Algorithm 1, we have Algorithm 2 to estimate the heat kernel $p_t^M(x, y)$.

Algorithm 2. estimate of the heat kernel by ball Algorithm

given $x, y \in M, t > 0, m, N \in \mathbb{N}, \epsilon > 0$, compute $V = \text{Vol}(\{z \in M : d(z, y) \leq \epsilon\})$;
 set $k = 0$;
 For $i = 1, \dots, N$
 sample a Brownian motion $B_x(\tau)$ for $\tau \in [0, t]$ starting from x by Algorithm 1;
 set $z = B_x(t)$;
 If $d(y, z) < \epsilon$
 set $k = k + 1$;
 set $p = \frac{k}{NV} \cdot \{ \text{an estimate of } p_t^M(x, y) \}$

3.2. Strip algorithm

In this subsection we will discuss an accelerated algorithm for an estimate of the heat kernel on a given manifold. We call it the strip method. Suppose that M is a Riemannian manifold of dimension m . We denote by $d(x, y)$ the geodesic distance between $x, y \in M$, i.e., the minimum of lengths of piecewise smooth curves on M connecting x and y . We define for each $x \in M, d_0 \geq 0, \epsilon > 0$ the set

$$S_x(d_0, \epsilon) := \{z \in M : |d(x, z) - d_0| < \epsilon\}$$

We also denote by $S_x(d_0)$ the set consisting of all $z \in M$ such that $d(x, z) = d_0$. From now on, we call $S_x(d_0, \epsilon)$ the ϵ -strip of $S_x(d_0)$. It is tempting to think $S_x(d_0, \epsilon)$ as the tube of $S_x(d_0)$ of radius ϵ . This is not always the case, but it is true with a minor assumption on M , which is obviously satisfied by manifolds we considered in this paper. We refer readers to Lemma D.1 in Appendix for the description of this minor assumption. Moreover, we prove in Lemma D.2 in Appendix that $S_x(d_0)$ is a closed submanifold of M for most choices of d_0 . Hence we may apply Theorem D.3 in Appendix to estimate the volume of the tube $S_x(d_0, \epsilon)$.

We assume that the heat kernel $p_t^M(x, y)$ is a function of distance at some $x \in M$, i.e.,

$$p_t^M(x, y_1) = p_t^M(x, y_2), \quad \text{whenever } d(x, y_1) = d(x, y_2). \quad (8)$$

Manifolds satisfying (8) include Euclidean spaces, spheres, projective spaces and their quotients. For such a manifold, we have the following analogue of (7):

$$p_t^M(x, y) \approx \frac{1}{\text{Vol}(S_x(d_0, \epsilon))} \frac{k}{N}, \quad (9)$$

where $d_0 = d(x, y)$, N is the total number of sampling Brownian paths starting from x on M and k is the number of Brownian paths falling into $S_x(d_0, \epsilon)$ at time t . From (9) we obtain Algorithm 3 for the estimate of the heat kernel on a manifold satisfying property (8). Once we have the point estimates of $p_t^M(x, y)$ for some pairs of (x, y) , we can use some standard interpolation methods to learn $p_t^M(x, y)$ as a function of distance.

Algorithm 3. estimation of heat kernel on a manifold by strip algorithm
 given $x \in M, d_0 > 0, t > 0, m, N \in \mathbb{N}, \epsilon > 0$, compute $V = \text{Vol}(S_x(d_0, \epsilon))$;
 set $k = 0$;
 For $i = 1, \dots, N$
 sample a Brownian path $B_x(\tau)$ for $\tau \in [0, t]$ starting from x by Algorithm 1;
 set $z = B_x(t)$;
 If $d(x, z) < d_0 + \epsilon$ and $d_0 - \epsilon < d(x, z)$
 set $k = k + 1$;
 set $p = \frac{k}{NV}$. {an estimate of $p_t^M(x, y)$ for any (x, y) with $d(x, y) = d_0$ }

The idea behind the strip method is similar to that of the ball method: if we treat the strip as a collection of many small balls, then the transition probability for the strip would approximately be the sum of the transition probability for these balls. Moreover, the transition density is calculated as the ratio of the transition probability and the strip volume. An illustrative diagram is shown in Figure 1(b). For a fixed $x \in M$, if $p_t^M(x, y)$ does not satisfy (8), then Algorithm 3 estimates the average density of $p_t^M(x, y)$ on $S_x(d_0, \epsilon)$. To be more precise, we have

$$\frac{1}{\text{Vol}(S_x(d_0, \epsilon))} \int_{S_x(d_0, \epsilon)} p_t^M(x, y) dy \approx \frac{1}{\text{Vol}(S_x(d_0, \epsilon))} \frac{k}{N},$$

where k, N and $\text{Vol}(S_x(d_0, \epsilon))$ are the same as those appeared in (9).

To conclude this subsection, we remark that Algorithm 2 requires the computation of the volume of the strip $S_x(d_0, \epsilon)$. For readers' convenience, we record formulae for the volume of a tube on some Riemannian manifolds in Appendix D.

3.3. Comparison of Ball Algorithm and Strip Algorithm

It is clear that Algorithm 2 is applicable to a more general class of manifolds than Algorithm 3, since Algorithm 3 can only be applied to M where $p_t^M(x, y)$ only depends on $d(x, y)$ if we fix

Table 1. Heat kernels of manifolds discussed in this paper

	Closed formula	Ball method	Strip method
Euclidean space	yes	yes	yes
(special) orthogonal/unitary group	no	yes	no
sphere	no	yes	yes
Stiefel manifold	no	yes	no
real projective space	no	yes	yes
complex projective space	no	yes	yes
Grassmannian	no	yes	no

t and $x \in M$. Table 1 gives a list of manifolds to be discussed in Section 4 together with the applicability of the two methods to these manifolds.

The closed formulas of heat kernel are only available for Euclidean space and real hyperbolic space. Here the ‘‘closed formula’’ means analytic expression. The power series expression of the heat kernel may exist for some manifolds such as sphere. The ball algorithm is applicable for all manifolds considered in this paper. The strip algorithm is only applicable for some in the list. However, when both algorithms are applicable, intuitively Algorithm 3 is more efficient than Algorithm 2, in the sense that Algorithm 3 requires fewer Brownian motion sample paths to estimate the heat kernel. In other words, a lot more sample paths need to be simulated to reach the ‘ball’ than the ‘strip’. For concrete examples, we compare in Figure 3 the two algorithms on \mathbb{R}^n for $n = 1, 2, 3$ respectively. By using the same number of Brownian motion sample paths, the strip algorithm outperforms the ball algorithm as the dimension of M increases. Theorem 2 below explains why the strip method is much more efficient.

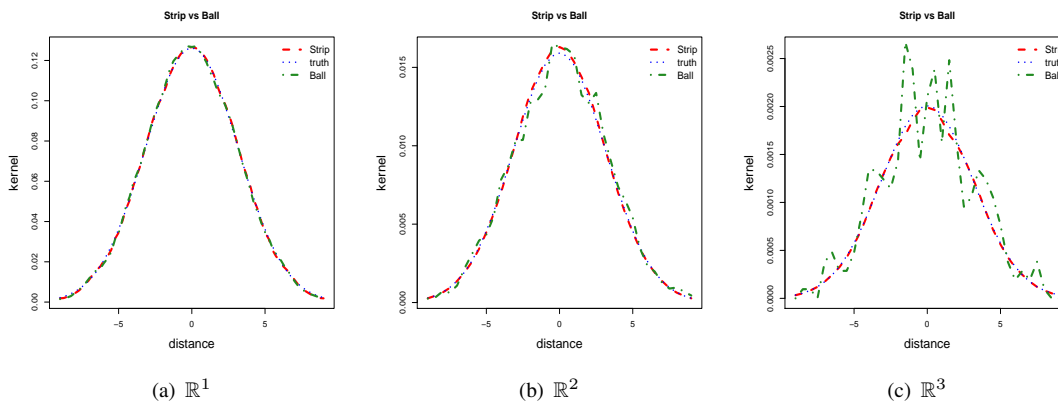


Fig. 2. Comparison of the estimate of heat kernel on \mathbb{R}^1 , \mathbb{R}^2 and \mathbb{R}^3 using strip and ball algorithms. The number of Brownian motion sample paths are 20000 for all three cases. The same window size and strip width are used. The true kernel values are plotted in dotted blue line while the estimations from ball algorithm are in green dot-dash line and strip method are in red dash line.

THEOREM 2. *Let M be a Riemannian manifold of dimension m and let $x_0, y_0 \in M$ be fixed points with distance $d_0 = d(x_0, y_0)$. Suppose that $p_t^M(x_0, y)$ satisfies (8). Then for any $a > 0$*

there exists some $\epsilon_0 > 0$ such that for each $0 < \epsilon \leq \epsilon_0$,

$$\frac{\mathbb{P}\{B_{x_0}(t) \in S_{x_0}(d_0, \epsilon)\}}{\mathbb{P}\{B_{x_0}(t) \in D(y_0, \epsilon)\}} \approx \frac{\text{Vol}(S_{x_0}(d_0, \epsilon))}{\text{Vol}(D(y_0, \epsilon))} \geq \frac{\pi^{\frac{-m+1}{2}} (\frac{1}{2}m)!}{(1+a)^2 (\frac{1}{2})!} \epsilon^{-m+1}, \quad (10)$$

where $B_{x_0}(t)$ is the point at time t on a Brownian motion sample path starting from x_0 and $D(y_0, \epsilon)$ is the set of points on M whose distance to y_0 is at most ϵ .

Proof. The equality in (10) follows from the relation between the heat kernel and Brownian motion, i.e.,

$$\mathbb{P}\{B_x(t) \in D\} = \int_D p_t^M(x, y) dy$$

and the assumption (8). The inequality is obtained from Theorem D.3. \square

We remark that the lower bound in (10) is not sharp. For example, in one dimensional case we have

$$\frac{\mathbb{P}\{B_{x_0}(t) \in S_{x_0}(d_0, \epsilon)\}}{\mathbb{P}\{B_{x_0}(t) \in D(y_0, \epsilon)\}} \approx \frac{\text{Vol}(S_{x_0}(d_0, \epsilon))}{\text{Vol}(D(y_0, \epsilon))} \geq \frac{1}{(1+a)^2}.$$

If $M = \mathbb{R}$ or S^1 , then it is straightforward to verify that

$$\frac{\mathbb{P}\{B_{x_0}(t) \in S_{x_0}(d_0, \epsilon)\}}{\mathbb{P}\{B_{x_0}(t) \in D(y_0, \epsilon)\}} = 2 > \frac{1}{(1+a)^2}.$$

However, if ϵ is small, the lower bound in (10) is already an exponential function in n . Hence we can conclude that Algorithm 3 is exponentially more efficient than Algorithm 2. In other words, (10) implies that if we fix the number of sampling Brownian paths, then the number of paths falling into the strip $S_{x_0}(d_0, \epsilon)$ is much more than the number of paths falling into the ball $D(y_0, \epsilon)$. To conclude this section, we remark that Niu et al. (2018) has proved the estimator of heat kernel in the ball algorithm is asymptotically unbiased and consistent. Following the similar idea, it is straight forward to prove that the estimator of heat kernel in the strip algorithm is also asymptotically unbiased and consistent.

4. HEAT KERNEL ON MANIFOLDS

In this section, we develop explicit algorithms to simulate the Brownian motion on orthogonal groups, unitary groups, Stiefel manifolds and Grassmannian manifolds. Readers who are not familiar with those manifolds can find basic facts about matrix Lie groups in Appendix A and about Stiefel manifolds and Grassmannian manifolds in Appendix B. Before we proceed, we want to point out that although algorithms presented in this section are obtained in essence from Algorithms 1, efficient numerical computations on each of those specific manifolds depend heavily on their geometric structures. To avoid distracting readers with too many algorithms, we record our Algorithms 4–8 in Appendix E. Moreover, with these Algorithms in hand, we can apply Algorithms 2 and 3 to estimate heat kernels on these manifolds efficiently.

4.1. Brownian motion on $O(n)$, $SO(n)$, $U(n)$ and $SU(n)$

We notice by Table 4 that $O(n)$ is a disconnected manifold, whose identity component is $SO(n)$. Therefore, it is sufficient to simulate the Brownian motion on $SO(n)$. By Equation (A9) in Appendix, geodesic curves on $SO(n)$ are explicitly known, Algorithm 1 can be applied directly. We recall that by Equation (A7) the tangent space of $SO(n)$ at $A \in SO(n)$

is simply a left translation of $\mathfrak{o}(n)$ by A , where $\mathfrak{o}(n)$ is the space of $n \times n$ skew symmetric matrices. Moreover, since $\mathfrak{o}(n)$ is a vector space, a Brownian path $W(t)$ in $\mathfrak{o}(n)$ is of the form $W(t) = (W_{ij}(t))$ where $W_{ii}(t) = 0, i = 1, \dots, n$, $W_{ij}(t)$ is a Brownian path on \mathbb{R} and $W_{ji}(t) = -W_{ij}(t), 1 \leq i < j \leq n$.

On $U(n)$ (resp. $SU(n)$), the algorithm for the simulation of the Brownian motion sample paths is similar. We simply replace the Brownian motion sample path $W(t) \in \mathfrak{o}(n)$ in Algorithm 4 by a Brownian motion sample path in $\mathfrak{u}(n)$ (resp. $\mathfrak{su}(n)$).

4.2. Brownian motion on Stiefel manifold

For notational simplicity, we will only discuss the real Stiefel manifolds, as the case of complex Stiefel manifolds is exactly the same. To begin with, we recall that given positive integers $k \leq n$, the Stiefel manifold over \mathbb{R} is defined as

$$V_{\mathbb{R}}(k, n) := \{A \in \mathbb{R}^{n \times k} : A^T A = I_k\}.$$

In particular, if $k = 1$ then $V_{\mathbb{R}}(k, n)$ is simply the $(n - 1)$ -dimensional sphere \mathbb{S}^{n-1} . For instance,

$$V_{\mathbb{R}}(1, 2) = \mathbb{S}^1 = \{(\cos \theta, \sin \theta)^T : \theta \in [0, 2\pi)\}.$$

Another extreme example is $k = n$, in which case $V_{\mathbb{R}}(k, n)$ is the orthogonal group $O(n)$ discussed in Section 4.1.

To estimate the heat kernel on $V_{\mathbb{R}}(k, n)$, we need to compute the distance between $A, B \in V_{\mathbb{R}}(k, n)$, which amounts to find $X \in T_A V_{\mathbb{R}}(k, n)$ such that the geodesic determined by A and X also passes through B . Indeed, according to equation (A5), X can be calculated by solving the system:

$$B = AM + QN, \quad (11)$$

$$QR = (I_n - AA^T)X, \quad (12)$$

$$\begin{bmatrix} M \\ N \end{bmatrix} = \exp \left(\begin{bmatrix} A^T X & -R^T \\ R & 0 \end{bmatrix} \right) I_{2k,k}, \quad (13)$$

where Q is a $n \times k$ matrix such that $Q^T Q = I_k$ and R is a $k \times k$ upper triangular matrix. In general, the system (11)-(13) has no explicit solution, but one can solve it explicitly if $k = 1$, as we will see in Proposition A1. According to Algorithm 1, we need two ingredients to simulate Brownian paths on a Stiefel manifold $V_{\mathbb{R}}(k, n)$: Brownian paths on the tangent space $T_A V_{\mathbb{R}}(k, n)$ and the geodesic curve passing through A with tangent direction $X \in T_A V_{\mathbb{R}}(k, n)$. To do concrete computations, we write an element $A \in V_{\mathbb{R}}(k, n)$ as an $n \times k$ matrix such that $A^T A = I_k$, rather than an equivalence class of an orthogonal matrix in the quotient $SO(n)/SO(n-k)$. Although (A6) provides us an explicit expression for geodesics, it is not obvious how we could simulate Brownian paths on $T_A V_{\mathbb{R}}(k, n) = \{\Delta \in \mathbb{R}^{n \times k} : A^T \Delta + \Delta^T A = 0\}$ for arbitrary $A \in V_{\mathbb{R}}(k, n)$. To this end, we first observe that

$$T_{I_{n,k}} V_{\mathbb{R}}(k, n) = \left\{ \begin{bmatrix} \Delta_1 \\ \Delta_2 \end{bmatrix} : \Delta_1 \in \mathfrak{o}(k), \Delta_2 \in \mathbb{R}^{(n-k) \times k} \right\}. \quad (14)$$

More generally, Lemma A2 implies that at any point $A \in V_{\mathbb{R}}(k, n)$, we could first simulate Brownian paths in $T_{I_{n,k}} V_{\mathbb{R}}(k, n)$, which is easy by (14), then multiply the Brownian path by some $Q \in SO(n)$ such that $Q I_{n,k} = A$ to obtain a Brownian path on $T_A V_{\mathbb{R}}(k, n)$. To summarize, we Algorithm 5 for simulations of Brownian motions on $V_{\mathbb{R}}(k, n)$.

We notice that if $k = 1$, Algorithm 5 can be simplified. Indeed, we have

$$X_{i,\delta}(\delta) = \begin{bmatrix} 0 \\ \epsilon_2 \\ \vdots \\ \epsilon_n \end{bmatrix}, \quad R = \sqrt{\sum_{j=2}^n \epsilon_j^2}, \quad Q = R^{-1} Q_{i-1} X_{i,\delta}(\delta) \quad (15)$$

and $M = \cos R, N = \sin R$, which implies

$$A_i = A_{i-1} \cos R + R^{-1} Q_{i-1} X_{i,\delta}(\delta) \sin R. \quad (16)$$

Combining the above calculation with Algorithm 5, we obtain Algorithm 6.

4.3. Brownian motion on Grassmannian manifolds

Let \mathbb{F} be \mathbb{R} or \mathbb{C} . Given positive integers $k \leq n$, the Grassmannian manifold $\text{Gr}_{\mathbb{F}}(k, n)$ is defined by

$$\text{Gr}_{\mathbb{F}}(k, n) := \{A \in \mathbb{F}^{n \times n} : A^* = A^2 = A, \text{rank}(A) = k\}.$$

Here X^* denotes the conjugate transpose of a matrix X . In particular, $\mathbb{P}_{\mathbb{F}}^{n-1} := \text{Gr}_{\mathbb{F}}(1, n)$ is called the $(n-1)$ -dimensional projective space over \mathbb{F} . According to the definition, $\mathbb{P}_{\mathbb{F}}^{n-1}$ consists of all $n \times n$ matrices A which can be written as $A = uu^*$, where u is a unit column vector of dimension n . For instance, if $n = 2$ and $\mathbb{F} = \mathbb{R}$, then we can write $u = (\cos \theta, \sin \theta)^{\top} \in \mathbb{R}^2$ and we have

$$\mathbb{P}_{\mathbb{R}}^1 = \left\{ \begin{bmatrix} \cos^2 \theta & \cos \theta \sin \theta \\ \cos \theta \sin \theta & \sin^2 \theta \end{bmatrix} : \theta \in [0, 2\pi) \right\}. \quad (17)$$

Another example is for $n = 2$ and $\mathbb{F} = \mathbb{C}$. In this case, we have $u = (\cos \theta e^{i\phi}, \sin \theta e^{i\psi}) \in \mathbb{C}^2$ with $\theta \in [0, \pi/2], \phi, \psi \in [0, 2\pi)$ and

$$\mathbb{P}_{\mathbb{C}}^1 = \left\{ \begin{bmatrix} \cos^2 \theta & \cos \theta \sin \theta e^{i(\phi-\psi)} \\ \cos \theta \sin \theta e^{i(\psi-\phi)} & \sin^2 \theta \end{bmatrix} : \theta \in [0, \pi/2], \phi, \psi \in [0, 2\pi) \right\}. \quad (18)$$

In general, $\text{Gr}_{\mathbb{F}}(k, n)$ does not admit a simple parametrisation like (17) and (18), but there are several convenient ways to describe a point in $\text{Gr}_{\mathbb{F}}(k, n)$.

Let $k \leq n$ be two non-negative integers and let \mathbb{A} be a point in $\text{Gr}_{\mathbb{F}}(k, n)$, i.e., a k -dimensional linear subspace of \mathbb{F}^n . We denote by $Y_{\mathbb{A}}$ an $n \times k$ matrix whose column vectors form an orthonormal basis of \mathbb{A} . According to Appendix B.2, the geodesic starting from \mathbb{A} with tangent direction $\Delta \in T_{\mathbb{A}} \text{Gr}_{\mathbb{F}}(k, n) = \{\Delta \in \mathbb{F}^{n \times k} : Y_{\mathbb{A}}^{\top} \Delta = 0\}$ is represented by the curve

$$Y(t) = [Y_{\mathbb{A}} V U] \begin{bmatrix} \cos \Sigma t \\ \sin \Sigma t \end{bmatrix} V^* \quad (19)$$

in $V_{\mathbb{F}}(k, n)$. Here $U \Sigma V^*$ is the compact singular value decomposition of Δ . Moreover, we notice that if $Y_{\mathbb{A}}^{\perp}$ is any $n \times (n-k)$ matrix whose column vectors form an orthonormal basis of the complement of \mathbb{A} in \mathbb{F}^n , then $\Delta \in T_{\mathbb{A}} \text{Gr}_{\mathbb{F}}(k, n)$ can also be written as

$$\Delta = Y_{\mathbb{A}}^{\perp} H, \quad H \in \mathbb{F}^{(n-k) \times k}. \quad (20)$$

We write diagonal entries of Σ as $\sigma_1, \dots, \sigma_k$ and we have Algorithm 7 to simulate a Brownian path on $\text{Gr}(k, n)$ starting from \mathbb{A} .

We remark that $\text{Gr}_{\mathbb{F}}(1, n)$ is of particular interest since in this case we have $\text{Gr}_{\mathbb{F}}(1, n) = \mathbb{P}_{\mathbb{F}}^{n-1}$. We recall from equation (26) in Appendix that $\mathbb{P}_{\mathbb{R}}^{n-1}$ is simply the quotient of \mathbb{S}^{n-1} by

a \mathbb{Z}_2 -action. Hence the heat kernel on $\mathbb{P}_{\mathbb{R}}^{n-1}$ can be efficiently estimated by the combination of Algorithm 6 and equation (29) in Appendix. The case of $\mathbb{P}_{\mathbb{C}}^{n-1}$ is more subtle. According to equation (27) in Appendix, we have that $\mathbb{P}_{\mathbb{C}}^{n-1}$ is the quotient of \mathbb{S}^{2n-1} by an action of \mathbb{S}^1 . Hence we have an integral formula Elworthy (1982); Ndumu (1996) for the heat kernel on $\mathbb{P}_{\mathbb{C}}^{n-1}$. It turns out that this integral formula is not practically useful. To this end, we may specialize Algorithm 7 to obtain Algorithm 8 for the simulation of Brownian paths starting from a fixed $[v]$ on $\mathbb{P}_{\mathbb{C}}^{n-1}$, where $[v]$ denotes the line in \mathbb{C}^n uniquely determined by the unit norm vector $v \in \mathbb{S}^{2n-1} \subseteq \mathbb{C}^n \setminus \{0\}$.

5. REGRESSION EXAMPLES

In this section, we carry out simulation studies for regression models with true regression functions defined on torus knots and high dimensional projective spaces. The performance of the intrinsic Gaussian process is compared with the extrinsic Gaussian process Lin et al. (2018), which is the euclidean Gaussian process using RBF kernel with embedding. To estimate intrinsic heat kernels in the two examples, we apply Algorithm 6 to simulate the Brownian motion on torus knots in Section 5.1 and we apply Algorithm 8 to simulate the Brownian motion on an eight dimensional projective spaces in Section 5.2.

5.1. Torus knots

The circle has a family of embeddings into \mathbb{R}^3 , whose images are torus knots indexed by a pair of coprime positive integers (p, q) . The explicit embedding associated to (p, q) can be found in standard textbooks in knots such as Milnor (1968); Rolfsen (2003); Murasugi (2007). In particular, we considered regression problems on three types of torus knots $(p = 2, q = 3)$, $(p = 4, q = 3)$ and $(p = 9, q = 8)$. As submanifolds of \mathbb{R}^3 , torus knots of different types are twisted in dramatically different ways. For example, readers can find pictures of torus knots of types mentioned above in Figure 3. We will see below by examples in Figure 3 that our intrinsic method is not affected by these twists while the extrinsic method does depend on them deeply.

The regression function on the torus knots is defined as

$$Y = X^T \mathcal{M} X + \epsilon, \quad (21)$$

where \mathcal{M} is a fixed 2×2 real positive definite matrix, X is a 2-dimensional unit norm real vector and ϵ is a i.i.d noise. The true function on the three type of torus knots are plotted in Figure 3(a) 3(d) and 3(g).

The intrinsic Gaussian process approach is compared with the extrinsic approach by embedding torus knots in \mathbb{R}^3 . On the one hand, the predictive means of the Gaussian process with embedding which is equivalent to using the Euclidean Gaussian process with RBF kernel in \mathbb{R}^3 is shown in Figure 3(b), 3(e) and 3(h). It is clear that the prediction from the Gaussian process with embedding does not agree with the truth when the crossing number increases. On the other hand, the predictive means of intrinsic Gaussian process in Figure 3(c), 3(f) and 3(i), which uses Algorithm 2 and Algorithm 6, recovers the true function very well. The numerical comparison is shown in Table 2. The root mean-squared errors (RMSE) are computed for the true function and the predictive means over 10 datasets. The mean and standard deviation (values in brackets) of RMSE are listed for both methods in different Torus knots. The prediction of in-GP is significantly better than the Euclidean GP with embedding.

Table 2. *Comparison of the RMSE of predictive means of two methods on Torus knots*

	GP embedding RBF kernel	Intrinsic GP
knot(2,3)	0.103 (0.014)	0.072 (0.01)
knot(4,3)	1.78(0.58)	0.072 (0.01)
knot(9,8)	2.29(0.75)	0.072 (0.01)

Table 3. *The comparison of the RMSE of predictive means of in-GP and Euclidean GP with different embeddings*

GP embedding RBF kernel	GP scaling embedding RBF kernel	GP embedding multiply matrix RBF kernel	Intrinsic GP
1.12(0.047)	1.39(0.02)	1.2(0.22)	0.69(0.025)

5.2. Projective spaces

In this section, we consider a higher dimensional example in the projective spaces $\mathbb{P}_{\mathbb{C}}^{n-1}$ which is defined and discussed in Section 4.3 and Appendix B.2. In particular, we consider regression problems on $\mathbb{P}_{\mathbb{C}}^4$ which is a 8-dimensional manifold. The intrinsic Gaussian process approach is compared with the extrinsic approach by embedding $\mathbb{P}_{\mathbb{C}}^4$ into \mathbb{R}^{25} . We recall from Section 4.3 that there is a classical embedding of $\mathbb{P}_{\mathbb{C}}^4$ given by

$$\iota_4 : \mathbb{P}_{\mathbb{C}}^4 \rightarrow \mathbb{C}^{5 \times 5}, \quad [u] \mapsto u^T u,$$

where u is a unit row vectors in \mathbb{C}^5 representing an element in $\mathbb{P}_{\mathbb{C}}^4$. The image of ι_4 lies in the vector space $V \subseteq \mathbb{C}^{5 \times 5}$ consisting of all Hermitian matrices and $\dim_{\mathbb{R}} V = 25$. We refer readers to Nicolaescu (1996.) for more details of the embedding ι_4 and its generalizations.

A similar regression function is used as in (21). Namely, we consider the function

$$Y = X^* \mathcal{M} X + \epsilon,$$

where X is a 5-dimensional unit norm complex column vector representing a point in $\mathbb{P}_{\mathbb{C}}^4$, \mathcal{M} is a randomly generated positive definite hermitian matrix, ϵ is a randomly generated error and X^* is the transpose conjugate of X . We also randomly generate 10 data points in $\mathbb{P}_{\mathbb{C}}^4$ and compute the corresponding Y . The comparison results of the root mean squared error (RMSE) of the prediction over 10 datasets using intrinsic approach and different types of embeddings are shown in Table 3. The first column is obtained by embedding $\mathbb{P}_{\mathbb{C}}^4$ via ι_4 into \mathbb{R}^{25} and using the RBF kernel; the second column is obtained by first embedding $\mathbb{P}_{\mathbb{C}}^4$ into \mathbb{R}^{25} via ι_4 and then multiplying the scalar 0.01; the third column is obtained by first embedding $\mathbb{P}_{\mathbb{C}}^4$ into \mathbb{R}^{25} via ι_4 and then multiplying a randomly generated 25×25 invertible real matrix; the last column is obtained by Algorithm 3 together with Algorithm 8, which does not depend on any embedding of $\mathbb{P}_{\mathbb{C}}^4$. Values in brackets are the standard deviations of RMSE. It is clear that the in-GP performs significantly better than extrinsic methods.

6. CONCLUSION

In this work, we propose a novel approach of constructing the intrinsic Gaussian process on manifolds such as orthogonal groups, unitary groups, Stiefel manifolds and Grassmannian manifolds. The heat kernel of a manifold is used as the covariance function of the intrinsic Gaussian

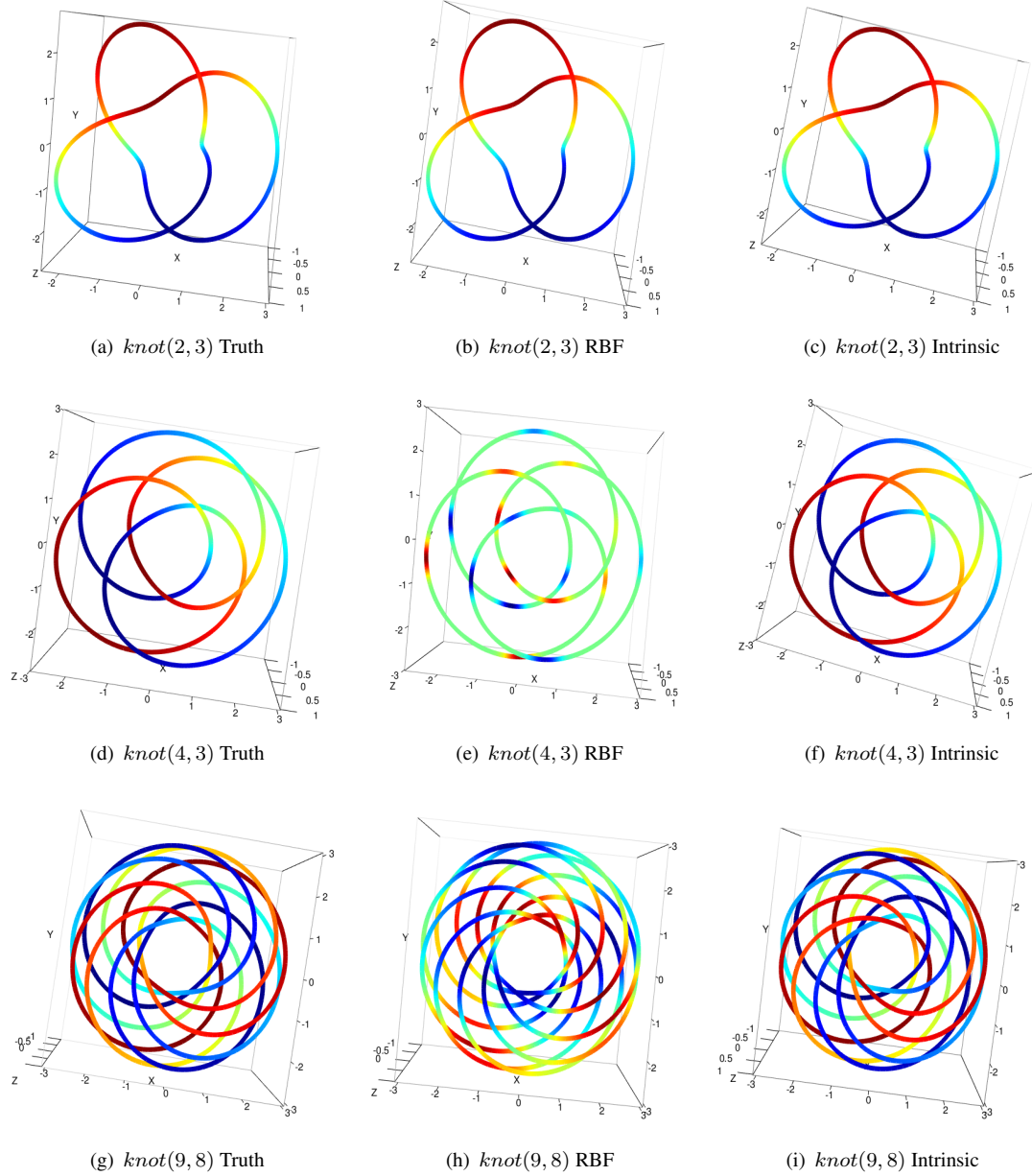


Fig. 3. Comparison of the truth and prediction using GP with RBF kernel embedded in R^3 and Intrinsic GP. The true value of the regression function is plotted in colour.

process, which can be estimated as the transition density of the Brownian motion on the manifold. The ball algorithm and the strip algorithm are developed to estimate the transition density of the Brownian motion. While the ball algorithm is applicable to a more general class of manifolds, the strip algorithm is proven to be more efficient, both mathematically and experimentally. We also compare the performance of the extrinsic method proposed in Lin et al. (2018) with that of our novel method on torus knots and high dimensional projective spaces. The compari-

son in section 5 indicates that the intrinsic Gaussian process achieves a significant improvement over the extrinsic Gaussian process. On the one hand, although there is an abundant interest in optimization on manifolds Absil et al. (2009); Boumal et al. (2014); Ring & Wirth (2012); Vandereycken (2013), we notice that most algorithms are based on the gradient descend method. On the other hand, the Bayesian optimization on Euclidean spaces is proven to be extremely effective in numerous scenarios. In future, we would like to combine these approaches with the intrinsic Gaussian process to perform the Bayesian optimisation on manifold.

SUPPLEMENTARY MATERIALS FOR HEAT KERNEL AND INTRINSIC GAUSSIAN PROCESSES ON MANIFOLDS

A. MATRIX LIE GROUPS

In this subsection, we will briefly review some basic facts about matrix Lie groups which we will use in this paper. Interested readers are referred to standard resources on differential geometry such as Helgason (2001), Lee (2012) and Warner (2013).

Let \mathbb{F} be either real or complex number field. We denote by $\mathbb{F}^{n \times n}$ the space of all $n \times n$ matrices over \mathbb{F} and we denote by $\text{GL}(n, \mathbb{F}) \subseteq \mathbb{F}^{n \times n}$ the group consisting of all invertible $n \times n$ matrices. Let G be a Lie subgroup of $\text{GL}(n, \mathbb{F})$ and let \mathfrak{g} be its Lie algebra. For each $A \in G$, the tangent space of G at A is

$$\tau_A G = A\mathfrak{g}. \quad (\text{A1})$$

Hence we may write a tangent vector of G at A as AX , where $X \in \mathfrak{g}$.

There is a canonical Riemannian metric g^c on G . To be more precise, we have a positive definite bilinear form g_A^c on $\tau_A G$ for each $A \in G$ defined by

$$g_A^c(AX, AY) = \text{tr}(X^*Y), \quad X, Y \in \mathfrak{g}, \quad (\text{A2})$$

and g_A^c varies smoothly with respect to A . For a given $X \in \mathfrak{g}$, we denote by $\|X\|$ the norm of X with respect to g^c , i.e.,

$$\|X\| := \sqrt{\text{tr}(X^*X)}. \quad (\text{A3})$$

It is clear that the metric g^c on G is bi-invariant if $G = \text{O}(n), \text{SO}(n), \text{U}(n)$ or $\text{SU}(n)$ where

1. general linear group: $\text{GL}(n, \mathbb{R}) := \{A \in \mathbb{R}^{n \times n} : \det(A) \neq 0\}$;
2. special linear group: $\text{SL}(n, \mathbb{R}) := \{A \in \text{GL}(n, \mathbb{R}) : \det(A) = 1\}$;
3. orthogonal group: $\text{O}(n) := \{A \in \text{GL}(n, \mathbb{R}) : A^T A = \text{I}_n\}$;
4. special orthogonal group: $\text{SO}(n) = \text{O}(n) \cap \text{SL}(n, \mathbb{R})$;
5. unitary group: $\text{U}(n) := \{A \in \text{GL}(n, \mathbb{C}) : A^* A = \text{I}_n\}$;
6. special unitary group: $\text{SU}(n) = \text{U}(n) \cap \text{SL}(n, \mathbb{C})$.

For instance, $\text{SO}(2)$ consists of all 2×2 matrices of the form

$$A = \begin{bmatrix} \cos \theta & \sin \theta \\ -\sin \theta & \cos \theta \end{bmatrix}, \quad \theta \in [0, 2\pi).$$

Correspondingly, the Lie algebra $\mathfrak{o}(2)$, which is defined to be the tangent space of $\text{SO}(2)$ at the identity $\text{I}_2 \in \text{SO}(2)$, consists of all 2×2 skew symmetric matrices, i.e.,

$$X = \begin{bmatrix} 0 & -a \\ a & 0 \end{bmatrix}, \quad a \in \mathbb{R}.$$

We summarize some important properties of these matrix Lie groups in Table 4.

Here $\mathfrak{so}(n)$ is the space of all skew-symmetric $n \times n$ real matrices; $\mathfrak{u}(n)$ is the space of all skew-Hermitian $n \times n$ complex matrices and $\mathfrak{su}(n)$ consists of all traceless skew-Hermitian $n \times n$ complex

Table 4. *topological properties of matrix Lie groups*

	connectedness	compactness	Lie algebra	dimension
$O(n)$	no	yes	$\mathfrak{so}(n)$	$n(n-1)/2$
$SO(n)$	yes	yes	$\mathfrak{so}(n)$	$n(n-1)/2$
$U(n)$	yes	yes	$\mathfrak{u}(n)$	n^2
$SU(n)$	yes	yes	$\mathfrak{su}(n)$	$n^2 - 1$

matrices. From now on, we assume that $G = O(n), SO(n), U(n)$ or $SU(n)$. With the canonical metric g^c , a geodesic curve $\gamma(t)$ passing through $A \in G$ with the tangent direction $AX \in \tau_A G$ is given by

$$\gamma(t) := A \exp(tX) = A \sum_{j=0}^{\infty} \frac{(tX)^j}{j!}. \quad (\text{A4})$$

The length of $\gamma(t) = A \exp(tX)$ is calculate by

$$L(\gamma) := \int_0^t \sqrt{g_{\gamma(s)}(\dot{\gamma}(s), \dot{\gamma}(s))} ds = t \|X\|. \quad (\text{A5})$$

LEMMA A1. *Let A, B be two points on $G = SO(n)$ or $SU(n)$ and let $\gamma(t)$ be the geodesic connecting A and B . The geodesic distance between A and B is*

$$d(A, B) = \sqrt{\sum_{j=1}^n |\log(\lambda_j)|^2}, \quad (\text{A6})$$

where $\lambda_1, \dots, \lambda_n$ are eigenvalues of A^*B and $\log(\lambda)$ is the principal logarithm of $\lambda \in \mathbb{C}$.

Proof. We only prove for $SO(n)$ as the proof for $SU(n)$ is similar. The Lie algebra of $SO(n)$ is

$$\mathfrak{so}(n) := \{X \in \mathbb{R}^{n \times n} : X^T + X = 0\}. \quad (\text{A7})$$

According to (A4), the geodesic passing through $A \in SO(n)$ with the tangent direction $AX \in \tau_A SO(n)$ is $\gamma(t) = A \exp(tX)$. If $\gamma(1) = B$, then $A^*B = \exp(X)$. Since X is a skew-symmetric matrix, the spectral theorem implies that

$$X = D^* \Sigma D, \quad (\text{A8})$$

where $D \in U(n)$ and Σ is a diagonal matrix whose diagonal entries are eigenvalues of X . Explicitly, we have

$$\Sigma = \begin{bmatrix} i\mu_1 & 0 & \cdots & 0 & 0 & 0 \cdots & 0 \\ 0 & -i\mu_1 & \cdots & 0 & 0 & 0 \cdots & 0 \\ \vdots & \vdots & \ddots & \vdots & \vdots & \vdots \ddots & \vdots \\ 0 & 0 & \cdots & i\mu_r & 0 & 0 \cdots & 0 \\ 0 & 0 & \cdots & 0 & -i\mu_r & 0 \cdots & 0 \\ 0 & 0 & \cdots & 0 & 0 & 0 \cdots & 0 \\ \vdots & \vdots & \ddots & \vdots & \vdots & \vdots \ddots & \vdots \\ 0 & 0 & \cdots & 0 & 0 & 0 \cdots & 0 \end{bmatrix},$$

where μ_1, \dots, μ_r are positive real numbers. Hence we may write the geodesic $\gamma(t)$ as

$$\gamma(t) = AU^* \exp(t\Sigma)U, \quad (\text{A9})$$

Moreover, we notice that X is in fact a real matrix, the norm of $X = D^* \Sigma D$ is

$$\|X\|_{\mathbb{R}} = \|\Sigma\|_{\mathbb{C}} = \sqrt{2 \sum_{j=1}^r \mu_j^2} = \sqrt{\sum_{j=1}^n |\log(\lambda_j)|^2}, \quad (\text{A10})$$

since $\|X\|_{\mathbb{R}}^2 = \text{tr}(X^T X) = \text{tr}(X^* X) = \|\Sigma\|_{\mathbb{C}}^2$. \square

Remark A1. Let \mathbb{F} be real or complex number field and let $X \in \mathbb{F}^{n \times n}$ be such that $X^* + X = 0$. Suppose $X = U^* \Sigma U$ is an eigendecomposition of X , where $U \in \text{U}(n)$ and Σ is a diagonal matrix whose diagonal entries are eigenvalues $\lambda_1, \dots, \lambda_n$ of X . Then the exponential $\exp(X)$ can be efficiently computed by

$$\exp(X) = U^* D U \quad (\text{A11})$$

where D is the diagonal matrix whose diagonal entries are $e^{\lambda_1}, \dots, e^{\lambda_n}$. If moreover we have $\text{tr}(X) = 0$, then nonzero eigenvalues of X must be of the form $\pm i\mu_1, \dots, \pm i\mu_r$ where $2r \leq n$. Hence $\exp(X)$ is calculated by

$$\exp(X) = U^* \begin{bmatrix} e^{i\mu_1} & 0 & \dots & 0 & 0 & 0 & \dots & 0 \\ 0 & e^{-i\mu_1} & \dots & 0 & 0 & 0 & \dots & 0 \\ \vdots & \vdots & \ddots & \vdots & \vdots & \vdots & \ddots & \vdots \\ 0 & 0 & \dots & e^{i\mu_r} & 0 & 0 & \dots & 0 \\ 0 & 0 & \dots & 0 & e^{-i\mu_r} & 0 & \dots & 0 \\ 0 & 0 & \dots & 0 & 0 & 1 & \dots & 0 \\ \vdots & \vdots & \ddots & \vdots & \vdots & \vdots & \ddots & \vdots \\ 0 & 0 & \dots & 0 & 0 & 0 & \dots & 1 \end{bmatrix} U. \quad (\text{A12})$$

B. HOMOGENEOUS SPACES

A homogeneous space is a quotient space G/H where G is a Lie group and H is a closed Lie subgroup of G . For each $A \in G$, we denote by $[A]$ the coset AH , which is an element in G/H . For simplicity, we assume that $G \subseteq \mathbb{R}^{n \times n}$ is a compact, semi-simple matrix Lie group. By definition, G acts transitively on G/H via the action:

$$G \times G/H \rightarrow G/H, \quad (B, [A]) \rightarrow [BA].$$

Hence for each $[A] \in G/H$, the tangent space of G/H at $[A]$ is:

$$\tau_{[A]} G/H = \text{Ag}/\mathfrak{h} = \{A(X + \mathfrak{h}) : X \in \mathfrak{g}\}.$$

Let g^c be the Riemannian metric defined in (A2) on G . There exists a linear subspace $\mathfrak{m} \subseteq \mathfrak{g}$ such that

$$T_{[A]} G/H \simeq \mathfrak{m}, \quad \mathfrak{g} = \mathfrak{m} \oplus \mathfrak{h}. \quad (\text{A1})$$

The geodesic γ passing through $[A] \in G/H$ with the tangent direction $X \in \mathfrak{m}$ is given by

$$\gamma(t) = [A \exp(tX)]. \quad (\text{A2})$$

B.1. Stiefel manifold

Let \mathbb{F} be real or complex number field. For each pair of positive integers $k < n$, we define the Stiefel manifold $V(k, n)$ of orthonormal k -frames in \mathbb{F}^n to be

$$V_{\mathbb{F}}(k, n) := \{A \in \mathbb{F}^{n \times k} : A^* A = I_k\}. \quad (\text{A3})$$

The tangent space of $V_{\mathbb{F}}(k, n)$ at $A \in V_{\mathbb{F}}(k, n)$ is

$$T_A V_{\mathbb{F}}(k, n) = \{\Delta \in \mathbb{F}^{n \times k} : A^* \Delta + \Delta^* A = 0\}.$$

We notice that $V_{\mathbb{R}}(k, n)$ (resp. $V_{\mathbb{C}}(k, n)$) is a homogeneous space, i.e., it is the quotient of $\text{SO}(n)$ (resp. $\text{SU}(n)$) by its subgroup $\text{SO}(n-k)$ (resp. $\text{SU}(n-k)$):

$$\begin{aligned} V_{\mathbb{R}}(k, n) &\simeq \text{O}(n)/\text{O}(n-k) \simeq \text{SO}(n)/\text{SO}(n-k), \\ V_{\mathbb{C}}(k, n) &\simeq \text{U}(n)/\text{U}(n-k) \simeq \text{SU}(n)/\text{SU}(n-k). \end{aligned}$$

The quotient map $q : \text{SO}(n) \rightarrow \text{SO}(n)/\text{SO}(n-k) \simeq V_{\mathbb{R}}(n, k)$ is simply given by $A \rightarrow AI_{n,k}$ where

$$I_{n,k} = \begin{bmatrix} I_k \\ 0 \end{bmatrix} \in \mathbb{R}^{n \times k}.$$

The quotient map $\text{SU}(n) \rightarrow \text{SU}(n)/\text{SU}(n-k) \simeq V_{\mathbb{C}}(n, k)$ is defined in the same way.

In particular, if $k = 1$, then $V_{\mathbb{R}}(k, n) \simeq \mathbb{S}^{n-1}$ and the map q under this identification becomes

$$q : \text{SO}(n) \rightarrow \mathbb{S}^{n-1}, \quad \pi(A) = Ae_1, \quad (\text{A4})$$

where $e_1 = (1, 0, \dots, 0)^\top$. The fiber of q is obviously homeomorphic to $\text{SO}(n-1)$ and hence q is a fibration of $\text{SO}(n)$ over \mathbb{S}^{n-1} whose typical fiber is $\text{SO}(n-1)$. Since $A \in \text{SO}(2)$ can be parametrized as

$$A = \begin{bmatrix} \cos \theta & \sin \theta \\ -\sin \theta & \cos \theta \end{bmatrix}$$

Hence it is straightforward to verify that $q : \text{SO}(2) \rightarrow \mathbb{S}^1$ is a homeomorphism.

By (Edelman et al., 1998, Section 2.4.1), the geodesic curve passing through $A \in V_{\mathbb{F}}(k, n)$ with the tangent direction $X \in {}_{\tau_A} V_{\mathbb{F}}(k, n)$ is

$$\gamma(t) = AM(t) + QN(t), \quad (\text{A5})$$

where $QR = (I_n - AA^\top)X$ is the QR-decomposition of $(I_n - AA^\top)X$ and $M(t)$ and $N(t)$ are $k \times k$ matrices determined by

$$\begin{bmatrix} M(t) \\ N(t) \end{bmatrix} = \exp\left(t \begin{bmatrix} A^\top X & -R^\top \\ R & 0 \end{bmatrix}\right) I_{2k,k}.$$

Here the Riemannian metric g^c equipped on $V_{\mathbb{F}}(k, n)$ is the canonical metric induced from the quotient space structure of $V_{\mathbb{F}}(k, n)$. To be more precise,

$$g_A^c(\Delta, \Delta) := 2 \text{tr} \Delta^\top (I_n - AA^\top) \Delta.$$

With this canonical metric, it is straightforward to verify that a geodesic starting from $A \in V_{\mathbb{F}}(k, n)$ with the tangent direction $PX I_{n,k} \in {}_{\tau_A} V_{\mathbb{F}}(k, n)$ can also be written as

$$\gamma(t) = P \exp(tX) I_{n,k}, \quad (\text{A6})$$

where P is an orthogonal matrix (resp. unitary matrix) such that $PI_{n,k} = A$.

PROPOSITION A1. *Let γ be the geodesic curve starting from $A \in V_{\mathbb{R}}(k, n)$ with the direction $PX I_{n,k} \in {}_{\tau_A} V_{\mathbb{R}}(k, n)$ where P, X are as above. The length of γ is*

$$L(\gamma) = \sqrt{\int_0^\tau g_{\gamma(t)}^c(\gamma'(t), \gamma'(t)) dt} = \sqrt{-\text{tr}(Y^2) + 2 \text{tr}(ZZ^\top)} = \|X\|_F. \quad (\text{A7})$$

In particular, if we specialize to the case $k = 1$, then the geodesic curve connecting $A, B \in V(1, n) = \mathbb{S}^{n-1}$ is just the arc of the big circle from A to B and the geodesic distance between A and B is simply

$$d^c(A, B) = \theta, \quad (\text{A8})$$

where $\theta \in [0, \pi]$ is the angle between A and B , i.e., $\cos \theta = A^\top B$.

Proof. The first part follows directly from the definition of $L(\gamma)$ and g^c . Hence it is only left to prove the statement for $k = 1$. In this case, we notice that A, B are simply column vectors of dimension n . We let $\theta \in [0, \pi]$ be the angle between A and B . By definition of X , we must have $A^\top X = 0$ and the system equation (11)–(13) in the main paper reduces to

$$\begin{aligned} B &= mA + nQ, \\ rQ &= X, \\ \begin{bmatrix} m \\ n \end{bmatrix} &= \exp\left(\begin{bmatrix} 0 & -r \\ r & 0 \end{bmatrix}\right) \mathbf{I}_{2,1}, \end{aligned}$$

where m, n, r are real numbers and A, B, Q are unit column vectors of dimension n . Now it is straightforward to verify that $r = \theta$, $m = \cos \theta$, $n = \sin \theta$ and $\|X\|_F = \theta$. \square

LEMMA A2. *For any $Q \in \text{SO}(n)$ such that $Q \mathbf{I}_{n,k} = A$, we have*

$$\tau_A V_{\mathbb{R}}(k, n) = Q_{\tau \mathbf{I}_{n,k}} V_{\mathbb{R}}(k, n).$$

Proof. We notice that

$$\dim \tau_A V_{\mathbb{R}}(k, n) = \dim \tau_{\mathbf{I}_{n,k}} V_{\mathbb{R}}(k, n) = \dim Q_{\tau \mathbf{I}_{n,k}} V_{\mathbb{R}}(k, n).$$

Hence it is sufficient to prove that $Q_{\tau \mathbf{I}_{n,k}} V_{\mathbb{R}}(k, n) \subseteq \tau_A V_{\mathbb{R}}(k, n)$. To see this, we let $\Delta = \begin{bmatrix} \Delta_1 \\ \Delta_2 \end{bmatrix}$ be an element in $\tau_{\mathbf{I}_{n,k}} V_{\mathbb{R}}(k, n)$ and write $Q = [A \ A']$. Then we must have

$$A^\top Q \Delta = A^\top (A \Delta_1 + A' \Delta_2) = \Delta_1 \in \mathfrak{o}(k),$$

since $A^\top A = \mathbf{I}_k$ and $Q \in \text{SO}(n)$. Therefore, by definition of $\tau_A V_{\mathbb{R}}(k, n)$, we see that $Q \Delta \in \tau_A V_{\mathbb{R}}(k, n)$ and this completes the proof. \square

B.2. Grassmannian manifolds

Let k, n be two non-negative integers such that $k \leq n$. The Grassmannian manifold $\text{Gr}_{\mathbb{F}}(k, n)$ consisting of all k -dimensional linear subspaces of \mathbb{F}^n . Moreover, $\text{Gr}_{\mathbb{F}}(k, n)$ is a homogeneous space:

$$\text{Gr}_{\mathbb{R}}(k, n) \simeq \text{O}(n) / (\text{O}(k, n) \times \text{O}(n - k, n)) \simeq \text{V}(k, n) / \text{O}(k), \quad (\text{A9})$$

$$\text{Gr}_{\mathbb{C}}(k, n) \simeq \text{U}(n) / (\text{U}(k, n) \times \text{U}(n - k, n)) \simeq \text{V}_{\mathbb{C}}(k, n) / \text{U}(k), \quad (\text{A10})$$

Here $\text{O}(k, n) \times \text{O}(n - k, n)$ is embedded in $\text{O}(n)$ as a Lie subgroup via the embedding

$$j : \text{O}(k, n) \times \text{O}(n - k, n) \rightarrow \text{O}(n), \quad j(A_1, A_2) = \begin{bmatrix} A_1 & 0 \\ 0 & A_2 \end{bmatrix}.$$

Similarly, $\text{U}(k) \times \text{U}(n - k)$ is regarded as a Lie subgroup of $\text{U}(n)$ via the same map.

We remark that the diffeomorphism $\text{Gr}_{\mathbb{R}}(k, n) \simeq \text{V}_{\mathbb{R}}(k, n) / \text{O}(k)$ (resp. $\text{Gr}_{\mathbb{C}}(k, n) \simeq \text{V}_{\mathbb{C}}(k, n) / \text{U}(k)$) is based on the fact that every k -dimensional subspace of \mathbb{F}^n admits an orthonormal basis, which is unique up to a rotation. To be more precise, let \mathbb{A} be subspace in \mathbb{F}^n of dimension k and let v_1, \dots, v_k be an orthonormal basis. Then we have $V = [v_1, \dots, v_k] \in \text{V}_{\mathbb{F}}(k, n)$ and the column vectors of VQ also form an orthonormal basis of \mathbb{A} , for any $Q \in \text{O}(k)$ (resp. $Q \in \text{U}(k)$). Therefore, in the rest of this paper, we simply represent an element $\mathbb{A} \in \text{Gr}_{\mathbb{F}}(k, n)$ by an $n \times k$ matrix $Y_{\mathbb{A}} \in \text{V}_{\mathbb{F}}(k, n)$, whose column vectors form an orthonormal basis of \mathbb{A} . The tangent space of $\text{Gr}_{\mathbb{F}}(k, n)$ at \mathbb{A} is:

$$T_{\mathbb{A}} \text{Gr}_{\mathbb{F}}(k, n) = \{\Delta \in \mathbb{F}^{n \times k} : Y_{\mathbb{A}}^* \Delta = 0\} \quad (\text{A11})$$

The canonical metric on Stiefel manifolds we discussed in Section B.1 induces a Riemannian metric on $\text{Gr}(k, n)$ via its quotient space structure (A9) and (A10). Equipping with this induced metric, the geodesic curve emanating from $\mathbb{A} \in \text{Gr}_{\mathbb{F}}(k, n)$ with tangent direction $\Delta \in T_{\mathbb{A}} \text{Gr}_{\mathbb{F}}(k, n)$ is given by

$$\mathbb{A}(t) = \text{span} \left([Y_{\mathbb{A}} \ V \ U] \begin{bmatrix} \cos \Sigma t \\ \sin \Sigma t \end{bmatrix} V^\top \right), \quad (\text{A12})$$

where $U\Sigma V^\top$ is the compact singular value decomposition of Δ and $\text{span}(Y)$ means the linear subspace spanned by column vectors of a matrix Y . We refer interested readers to (Edelman et al., 1998, Section 2.5.1) for detailed computation of geodesic curves on $\text{Gr}_{\mathbb{F}}(k, n)$. Moreover, the geodesic distance between $\mathbb{A}, \mathbb{B} \in \text{Gr}(k, n)$ is simply

$$d^c(\mathbb{A}, \mathbb{B}) = \sqrt{\sum_{j=1}^k \theta_j^2}, \quad (\text{A13})$$

where $\cos(\theta_j)$ is the j -th singular value of $A^\top B$ and A (resp. B) is the $n \times k$ matrix such that $A^\top A = I_k$ (resp. $B^\top B = I_k$) representing \mathbb{A} (resp. \mathbb{B}).

In particular, $\text{Gr}_{\mathbb{R}}(1, n) \simeq \mathbb{P}_{\mathbb{R}}^{n-1}$, the $(n-1)$ -dimensional projective space over \mathbb{F} , consisting of all lines pass through the origin in \mathbb{F}^n . We remind the audiences who are not familiar with projective spaces that

$$\mathbb{P}_{\mathbb{R}}^{n-1} \simeq \mathbb{S}^{n-1}/\mathbb{Z}_2, \quad (\text{A14})$$

obtained from \mathbb{S}^{n-1} by identifying the antipodal points. Over \mathbb{C} , we have

$$\mathbb{P}_{\mathbb{C}}^{n-1} \simeq \mathbb{S}^{2n-1}/\mathbb{S}^1, \quad (\text{A15})$$

identifying $x \in \mathbb{S}^{2n-1} \subseteq \mathbb{C}^n$ with points in \mathbb{S}^{2n-1} of the form λx for $\lambda \in \mathbb{S}^1 \subseteq \mathbb{C}$. In this case, formula (A13) becomes

$$d^c(\mathbb{A}, \mathbb{B}) = |\theta|, \quad (\text{A16})$$

where $\theta = \arccos(A^*B) \in [-\pi/2, \pi/2)$ and A (resp. B) is an element in $V_{\mathbb{F}}(1, n)$ representing \mathbb{A} (resp. \mathbb{B}).

C. HEAT KERNEL ON A QUOTIENT MANIFOLD

Let M be a Riemannian manifold with metric g^M and let G be a group acting on M freely, properly and isometrically. Then we have Proposition A2, for which we give a proof here due the lack of appropriate reference, although this fact is well-known to the community of differential geometry.

PROPOSITION A2. *There exists a unique metric on the quotient manifold $X = M/G$ such that*

$$p^X(t, [x], [y]) = \int_G p^M(t, x, gy), \quad (\text{A1})$$

where $[x], [y]$ are points in X represented by $x, y \in M$ respectively. In particular, if G is a finite group, then

$$p^X(t, [x], [y]) = \sum_{g \in G} p^M(t, x, gy).$$

Proof. According to (Gallot et al., 1990, Proposition 2.20), there exists a unique metric on X , such that the quotient map $\pi : M \rightarrow M/G$ is a Riemannian covering map, i.e., π is a locally isometric smooth covering map. One can obtain (A1) by recalling the definition of the heat kernel. \square

D. TUBES ON A MANIFOLD

We summarize some facts about the volume of a tube on a manifold in this subsection. Suppose that M is a Riemannian manifold of dimension m . We define for each $x \in M$, $d_0 \geq 0, \epsilon > 0$ the set

$$S_x(d_0, \epsilon) := \{y \in M : |d(x, y) - d_0| < \epsilon\}.$$

We also denote by $S_x(d_0)$ the set consisting of all $y \in M$ such that $d(x, y) = d_0$.

LEMMA A3. *Let M be a complete Riemannian manifold and let $D := \sup_{x,y \in M} d(x,y)$ be the diameter of M . We suppose that M has the following property: for any $x, y \in M$ with $d := d(x,y) < D$ and any distance minimizing unit speed geodesic curve $\gamma : [0, d] \rightarrow M$ connecting x and y , there is some positive $\epsilon \leq D - d$ such that $\bar{\gamma}$ is also distance minimizing. Here $\bar{\gamma}$ is the unit speed geodesic curve determined by*

$$\bar{\gamma}|_{[0,d]} = \gamma, \quad \bar{\gamma}'(d) = \gamma'(d).$$

Then for sufficiently small $\epsilon > 0$, the strip $S_x(d_0, \epsilon)$ can be described as

$$S_x(d_0, \epsilon) = \{y \in M : d(y, S_x(d_0)) < \epsilon\}.$$

That is, $S_x(d_0, \epsilon)$ is the tube of $S_x(d_0)$ of radius ϵ .

Proof. We denote by N_ϵ the set consisting of $y \in M$ such that

$$d(y, S_x(d_0)) < \epsilon.$$

Given a point $y \in N_\epsilon$, we have by triangle inequality that

$$\begin{aligned} d(y, x) &\leq d(y, S_x(d_0)) + d(S_x(d_0), x) < \epsilon + d_0, \\ d_0 - \epsilon &\leq d(S_x(d_0), x) - d(y, S_x(d_0)) \leq d(y, x), \end{aligned}$$

which implies $N_\epsilon \subseteq S_x(d_0, \epsilon)$. For the other containment, we notice that if there exists some $y \in S_x(d_0, \epsilon) \setminus N_\epsilon$, then we must have

$$|d(x, y) - d_0| < \epsilon \leq d(y, S_x(d_0)).$$

We let $\gamma : [0, d(x, y)] \rightarrow M$ be a unit speed distance minimizing curve connecting x and y . By the assumption on M , we can find some $z \in S_x(d_0)$ such that $d(y, z) < \epsilon$, which contradicts the fact that

$$\epsilon \leq d(y, S_x(d_0)) \leq d(y, z).$$

Indeed, if $d_0 \leq d(x, y)$, then we simply take $z = \gamma(d_0)$ and we take $z = \bar{\gamma}(d_0)$ otherwise. \square

LEMMA A4. *The set $S_x(d_0, \epsilon)$ is an open submanifold of M . Moreover, for a generic d_0 the set $S_x(d_0)$ is a $(m-1)$ -dimensional closed submanifold of M . To be more precise, the set of $d_0 \in \mathbb{R}_+$ such that $S_x(d_0)$ is not smooth has measure zero.*

Proof. We consider the map $\varphi : M \rightarrow \mathbb{R}_+$ defined by $\varphi(y) = d(x, y)$. It is obvious that φ is a continuous function and we have $S_x(d_0, \epsilon) = \varphi^{-1}((d_0 - \epsilon, d_0 + \epsilon))$. This implies that $S_x(d_0, \epsilon)$ is an open subset of M and hence it is a submanifold.

Since φ is a smooth function from M to \mathbb{R}_+ , by Sard's theorem the set of critical values of φ is of measure zero. This implies the set $S_x(d_0, \epsilon) = \varphi^{-1}(d_0)$ is a smooth closed submanifold of M for all $d_0 \in \mathbb{R}_+ \setminus E$ where E is some measure zero subset. \square

Let P be a q -dimensional submanifold of a Riemannian manifold M . We denote by $\text{Vol}_P^M(\epsilon)$ the volume of the tube around P in M of radius $\epsilon > 0$. Then we have

THEOREM A1. (Gray, 2012, Theorem 9.23) *There is a power series expansion of $\text{Vol}_P^M(\epsilon)$ in ϵ :*

$$\text{Vol}_P^M(\epsilon) = \frac{(\pi\epsilon^2)^{\frac{1}{2}(m-q)}}{(\frac{1}{2}(m-q))!} \int_P (1 + A\epsilon^2 + B\epsilon^4 + O(\epsilon^6)) dP,$$

where A, B are quantities determined by the curvature of M , curvature of P and the second fundamental form of P in M , which are independent to ϵ .

Let λ be a constant number and let $K^m(\lambda)$ be a Riemannian manifold of dimension m whose sectional curvature is identically λ . We denote by $V_x^{K^m(\lambda)}(r)$ the volume of the geodesic ball around $x \in K^m(\lambda)$ of radius r .

THEOREM A2. (Gray, 2012, Corollary 3.18) Let r_0 be the distance from x to its cut locus on $K^m(\lambda)$. For any $0 < r \leq r_0$, we have

$$\text{Vol}_x^{K^m(\lambda)}(r) = \frac{2\pi^{m/2}}{\Gamma(\frac{m}{2})} \int_0^r \left(\frac{\sin(t\sqrt{\lambda})}{\sqrt{\lambda}} \right)^{m-1} dt. \quad (\text{A1})$$

COROLLARY A1. For any $r \in (0, \pi]$, we have

$$\text{Vol}_x^{\mathbb{S}^m}(r) = \frac{2\pi^{n/2}}{\Gamma(\frac{m}{2})} \int_0^r (\sin(t))^{m-1} dt. \quad (\text{A2})$$

In particular, for any $x \in \mathbb{S}^m$ and $d_0 \in [\epsilon, \pi - \epsilon]$ the volume of $S_x(d_0, \epsilon)$ is

$$\text{Vol}(S_x(d_0, \epsilon)) = \text{Vol}_x^{\mathbb{S}^m}(d_0 + \epsilon) - \text{Vol}_x^{\mathbb{S}^m}(d_0 - \epsilon) = \frac{2\pi^{m/2}}{\Gamma(\frac{n}{2})} \int_{d_0-\epsilon}^{d_0+\epsilon} (\sin(t))^{m-1} dt. \quad (\text{A3})$$

E. SUMMARY OF ALGORITHMS IN SECTION 4

In this section, we record all algorithms discussed in Section 4.

Algorithm 4. Simulation of Brownian paths on $\text{SO}(n)$

Initialize $A_0 = A$;

For $i = 1, 2, \dots$

 compute $X_{i-1}(\delta) \in \mathfrak{o}(n)$; { BM sample path in $\mathfrak{o}(n)$ with step variance δ }
 compute svd: $X_{i-1}(\delta) = D^* \Sigma D$; { see equation (8) in Appendix }
 set $A_i = A_{i-1} D^* \exp(\Sigma) D$;

Algorithm 5. Simulation of Brownian paths on $V_{\mathbb{R}}(k, n)$

Initialize $A_0 = A$.

For $i = 1, 2, \dots$

 find $Q_{i-1} \in \text{SO}(n)$ such that $Q_{i-1} I_{n,k} = A_{i-1}$;
 compute $X_{i-1}(\delta)$; { Brownian motion sample path in $T_{I_{n,k}} V_{\mathbb{R}}(k, n)$ with step variance δ , see (14) }
 compute M, N, Q for A_{i-1} and $Q_{i-1} X_{i-1}(\delta)$; { see equation (17) in Appendix }
 set $A_i = A_{i-1} M + Q N$;

Algorithm 6. Simulation of Brownian paths on \mathbb{S}^{n-1}

Initialize $A_0 = A$.

For $i = 1, 2, \dots$

 find $Q_{i-1} \in \text{SO}(n)$ such that $Q_{i-1} I_{n,1} = A_{i-1}$;
 sample random values $\epsilon_2, \dots, \epsilon_n$ from $N(0, \sigma^2 = \delta)$;
 set $X_{i-1}(\delta) = (0, \epsilon_2, \dots, \epsilon_n)^T$;
 compute R and Q ; { see (15) }
 compute A_i ; { see (16) }

REFERENCES

ABSIL, P.-A., MAHONY, R. & SEPULCHRE, R. (2009). *Optimization algorithms on matrix manifolds*. Princeton University Press.

Algorithm 7. Simulation of Brownian paths on $\text{Gr}_{\mathbb{F}}(k, n)$

Initialize $Y_0 = Y_{\mathbb{A}}$.

For $i = 1, 2, \dots$

find an orthogonal complement Y_{i-1}^{\perp} of Y_{i-1} ;

sample random values ϵ_{jl} from $N(0, \sigma^2 = \delta)$ for $1 \leq j \leq n - k, 1 \leq l \leq k$;

set $\Delta_{i-1} = Y_{i-1}^{\perp}(\epsilon_{jl})$;

compute compact svd: $\Delta_{i-1} = U\Sigma V^*$;

set $\Lambda = \text{diag}(\cos(\sigma_1), \dots, \cos(\sigma_k))$;

set $\Gamma = \text{diag}(\sin(\sigma_1), \dots, \sin(\sigma_k))$;

set $Y_i = [Y_{i-1} V U] \begin{bmatrix} \Lambda \\ \Gamma \end{bmatrix} V^*$;

Algorithm 8. Simulation of Brownian paths on $\mathbb{P}_{\mathbb{C}}^{n-1}$

initialize $v_0 = v$.

For $i = 1, 2, \dots$

find an orthogonal complement v_{i-1}^{\perp} of v_{i-1} ;

sample random values $\epsilon_j \in \mathbb{C}$ from $N(0, \sigma^2 = \delta)$ for $1 \leq j \leq n - 1$;

compute $R = \sqrt{\sum_{j=1}^{n-1} |\epsilon_j|^2}$;

set $v_i = \cos(R)v_{i-1} + \sin(R)R^{-1}v_{i-1}^{\perp}(\epsilon_j)$;

- BERLINE, N., GETZLER, E. & VERGNE, M. (2003). *Heat Kernels and Dirac Operators*. Grundlehren Text Editions. Springer Berlin Heidelberg.
- BOOKSTEIN, F. L. (2013). *The measurement of biological shape and shape change*, vol. 24. Springer Science & Business Media.
- BOUMAL, N., MISHRA, B., ABSIL, P.-A. & SEPULCHRE, R. (2014). Manopt, a matlab toolbox for optimization on manifolds. *The Journal of Machine Learning Research* **15**, 1455–1459.
- CASTILLO, I., KERKYACHARIAN, G. & PICARD, D. (2014). Thomas bayes walk on manifolds. *Probab. Theory Relat. Fields* **158**, 665710.
- CHIKUSE, Y. (2012). *Statistics on special manifolds*, vol. 174. Springer Science & Business Media.
- EDELMAN, A., ARIAS, T. A. & SMITH, S. T. (1998). The geometry of algorithms with orthogonality constraints. *SIAM journal on Matrix Analysis and Applications* **20**, 303–353.
- ELWORTHY, K. D. (1982). *Stochastic differential equations on manifolds*, vol. 70. Cambridge University Press.
- FLETCHER, P. T., LU, C. & JOSHI, S. (2003). Statistics of shape via principal geodesic analysis on lie groups. In *2003 IEEE Computer Society Conference on Computer Vision and Pattern Recognition, 2003. Proceedings.*, vol. 1. IEEE.
- GALLOT, S., HULIN, D. & LAFONTAINE, J. (1990). *Riemannian geometry*, vol. 3. Springer.
- GANGOLLI, R. (1964). On the construction of certain diffusions on a differentiable manifold. *Zeitschrift für Wahrscheinlichkeitstheorie und Verwandte Gebiete* **2**, 406–419.
- GIDSKEHAUG, A. (1976). Statistics on a sphere. *Geophysical Journal International* **45**, 657–676.
- GRAY, A. (2012). *Tubes*, vol. 221. Birkhäuser.
- HELGASON, S. (2001). *Differential geometry and symmetric spaces*, vol. 341. American Mathematical Soc.
- HSU, E. P. (2008). A brief introduction to Brownian motion on a Riemannian manifold. *Lecture Notes*.
- HSU, P. (1988). Brownian motion and Riemannian geometry. *Contemporary Mathematics* **73**, 95–104.
- JAYASUMANA, S., HARTLEY, R. & SALZMANN, M. (2016). Kernels on riemannian manifolds. In *Riemannian Computing in Computer Vision*. Springer, pp. 45–67.
- JAYASUMANA, S., HARTLEY, R., SALZMANN, M., LI, H. & HARANDI, M. (2013). Kernel methods on the riemannian manifold of symmetric positive definite matrices. In *Proceedings of the IEEE Conference on Computer Vision and Pattern Recognition*.
- KENDALL, D. G. (1977). The diffusion of shape. *Advances in applied probability* **9**, 428–430.
- KLOEDEN, P. E. & PLATEN, E. (1992). Higher-order implicit strong numerical schemes for stochastic differential equations. *Journal of Statistical Physics* **66**, 283–314.
- LAFFERTY, J. & LEBANON, G. (2005). Diffusion kernels on statistical manifolds. *Journal of Machine Learning Research* **6**, 129–163.
- LEE, J. (2012). *Introduction to Smooth Manifolds*, vol. 218. Springer Science & Business Media.

- LIN, L., MU, N., CHAN, P. & DUNSON, D. B. (2018). Extrinsic Gaussian processes for regression and classification on manifolds. *Bayesian Analysis* In press.
- McKEAN, H. J. et al. (1960). Brownian motions on the 3-dimensional rotation group. *Memoirs of the College of Science, University of Kyoto. Series A: Mathematics* **33**, 25–38.
- MILNOR, J. (1968). *Singular points of complex hypersurfaces*. Princeton University Press.
- MURASUGI, K. (2007). *Knot theory and its applications*. Springer Science & Business Media.
- NDUMU, M. N. (1996). An integral formula for the heat kernel of tubular neighborhoods of complete (connected) riemannian manifolds. *Potential Analysis* **5**, 311–356.
- NICOLAESCU, L. I. (1996.). *Lectures on the geometry of manifolds*. World Scientific Publishing Co., Inc., River Edge, NJ.
- NIU, M., CHEUNG, P., LIN, L., DAI, Z., LAWRENCE, N. & DUNSON, D. (2018). Intrinsic gaussian processes on complex constrained domains. *Journal of the Royal Statistical Society, Series B, preprint* <https://doi.org/10.1111/rssb.12320>.
- RASMUSSEN, C. E. (2004). *Gaussian Processes in Machine Learning*. Springer Berlin Heidelberg, pp. 63–71.
- RING, W. & WIRTH, B. (2012). Optimization methods on riemannian manifolds and their application to shape space. *SIAM Journal on Optimization* **22**, 596–627.
- ROLFSEN, D. (2003). *Knots and links*, vol. 346. American Mathematical Soc.
- TURAGA, P., VEERARAGHAVAN, A., SRIVASTAVA, A. & CHELLAPPA, R. (2011). Statistical computations on grassmann and stiefel manifolds for image and video-based recognition. *IEEE Transactions on Pattern Analysis and Machine Intelligence* **33**, 2273–2286.
- VANDEREYCKEN, B. (2013). Low-rank matrix completion by riemannian optimization. *SIAM Journal on Optimization* **23**, 1214–1236.
- WARNER, F. W. (2013). *Foundations of differentiable manifolds and Lie groups*, vol. 94. Springer Science & Business Media.

[Received on X January 2020. Editorial decision on X April 2020]